

Broadband Four Elements PIFA Array for Access-Point MIMO Systems

Erik Fritz-Andrade¹, Ricardo Gómez-Villanueva¹, José Alfredo Tirado-Méndez^{2, *}, Luis Alberto Vasquez-Toledo³, Arturo Rangel-Merino², and Hildeberto Jardón-Aguilar¹

Abstract—An antenna array formed by four PIFA elements located very close to each other, with low inter-element matching for MIMO applications is proposed. The antenna array consists of four F-inverted wideband radiators, with a fractional bandwidth around 56%, spaced one to each other by a very short distance ($< 0.065\lambda_0$) at a centre frequency of 2.55 GHz. The operational bandwidth goes from 1.88 to 3.15 GHz considering the $S_{ii} < -10$ dB at each port. Moreover, the coupling among ports reaches values below $S_{ij} < -10$ dB and getting values less than -30 dB at 1.8 GHz, just by employing an uncomplicated technique implemented by a neutralization line between elements. The antenna array gain goes from 2 dB to 6 dB over the operating bandwidth. Concerning MIMO figures of merit, the radiation pattern of each element is orthogonal to each other. The Envelope Correlation Coefficient is below 0.04 at the designed frequency, reaching a peak around 0.082 at 1.8 GHz, but still achieving the requirement for MIMO operation (less than 0.5). The Total Active Reflection Coefficient (TARC) is almost convergent at the design frequency, showing low dependence on random signals at different elements, and finally, the diversity gain reaches values close to 20 dB, making the array suitable for MIMO access point applications.

1. INTRODUCTION

Given the fast evolution of communication systems, the demand for higher data rates in a specific channel with limited bandwidth has increased in recent years. Therefore, many commercial applications with Multiple Inputs and Multiple Outputs (MIMO) have been developed, which are superior to systems with a Single Input and a Single Output (SISO) in terms of bit rate and reliability [1–3]. The main characteristics that highlight MIMO systems are (1) an increased spectral efficiency by using multiple antennas in the transmission and reception ends, and (2) an increase of the wireless channel capacity [4]. Both have been studied theoretically and experimentally, showing substantial improvements in data throughput and reliability when using several antennas in both sides of the system, even surrounded by rich scattering environments. These statements can be explained by considering that the multipath propagation can support several independent sub-channels [5].

Nevertheless, the performance of MIMO sub-channels is degraded if there is a high correlation among them caused by poor diversity in multipath propagation as well as elevated electromagnetic coupling among the elements of the MIMO array [4, 6, 7]. The correlation caused by propagation and mutual coupling is strongly dependent on the array geometry and becomes more pronounced as the inter-element distance is diminished [8, 9]. Hence, the correlation among MIMO sub-channels is a hot

Received 12 August 2020, Accepted 14 October 2020, Scheduled 28 October 2020

* Corresponding author: José Alfredo Tirado-Méndez (jtiradom@ipn.mx).

¹ Telecommunications Section, CINVESTAV-IPN, Av. IPN 2508, Mexico City, Mexico. ² SEPI-ESIME Zacatenco, Instituto Politécnico Nacional, Av. IPN S/N, San Pedro Zacatenco, Mexico City, Mexico. ³ Electrical Department, UAM-Iztapalapa, Av. San Rafael Atlixco 186, Mexico City, Mexico.

topic in communications, especially in handsets where space is considerably reduced, and radiators are closely placed to each other.

There are diverse studies that demonstrate that a highly mutual coupling among radiators has a significant degrading effect on the MIMO channel capacity [10–13]. In the same way, the radiation efficiency is also decreased because the impedance matching is affected by the same phenomenon [14].

Therefore, considering the drawbacks mentioned above, various works have been developed to reduce the mutual coupling among antennas. Many of the solutions are inherently narrowband, e.g., EBG structures [15, 16] used as electromagnetic walls, neutralization lines [17, 18] employed to modify the current distribution on the array surface, decoupling networks with lumped [19, 20] or distributed elements [21] to mismatch the undesired signals, defected structures on the ground plane of the array [22, 23] and parasitic elements between antennas [24, 25], both also employed as electromagnetic walls. The problem gets more complicated when one tries to decouple multiband or wideband multiport arrays, even more, when such an array has more than two radiators.

As general antenna theory explains, the electric parameters of an antenna can change when one body of any kind approaches the radiator. In antenna arrays, the proximity among elements plays a very important role in the desired performance. When two radiators are closely separated, the mutual electromagnetic coupling can provoke port mismatching, increase cross-polarization levels, reshape the radiations pattern, etc.

Certain solutions have been proposed using three radiators arrangements to overcome the difficulties expressed above. The array proposed in [26] has two symmetric elements placed on the borders of a substrate and one asymmetric element located in the centre, perpendicular to the others. The achieved bandwidth is very wide, but external baluns with high performance are needed to feed the symmetric elements in this large bandwidth, and they are not included in the antenna structure. The antenna proposed in [27] recovers the same idea of placing two symmetric elements on opposite sides and a different kind of radiator in the centre; however, this design is a narrowband solution. Both [26, 27] exemplify this technique where different types of radiators are used in a MIMO array to effectively reduce the coupling among them and to obtain radiation patterns that point to different directions, achieving spatial diversity.

In [28–30], four elements MIMO-antenna arrays are shown where terminated loads are included to cancel mutual coupling among elements, and even more radiators are discussed in [31], where the elements are excited by a set of reconfigurable feeding networks. In the case of four elements, a perpendicular arrangement may be employed [32], but this is not a viable solution for some communications devices where there is not enough space to accommodate perpendicular antennas. When four radiators are considered in the array, some works implement a decoupling technique between pairs of elements. However, this procedure turns the design significantly bulkier and complex in some setups [28]. More compact arrays are proposed in [29] and [30] where an asymmetric element is rotated around a central point to complete four elements in the array. In both cases, isolating walls among elements were used as a decoupling technique.

In this article, the concept of rotating an antenna element to obtain a four-element array is explored with a different approach; instead of using different kinds of radiators, antenna alike elements are employed and decoupled by using neutralization lines.

2. ANTENNA CONFIGURATION AND SIMULATION RESULTS

For demonstration purposes, the array was designed to operate at a centre frequency of 2.55 GHz. The first approach of the design of the antenna array is presented in Figure 1, and this will be developed to obtain a compact and high-performance configuration.

As observed in Figure 1, each PIFA element uses a wide feeding plate with a simple tapered profile that reduces the reactive load near the feeding point, which allows matching the radiator over a wider bandwidth, as proposed in [33]. The short-circuited wire is connected at one point where the port matching at the center frequency is the best for the current configuration. Due to the symmetry of the antenna, parameters $S_{ii} = S_{jj}$, $S_{12} = S_{14} = S_{23} = S_{34}$, $S_{13} = S_{24} = S_{31} = S_{42}$, then to simplify the visualization of results, just S_{11} , S_{12} , and S_{13} are described as shown in Figure 2.

As seen in Figure 2, the bandwidth of the antenna array shown is of 700 MHz, starting at 2.35 GHz

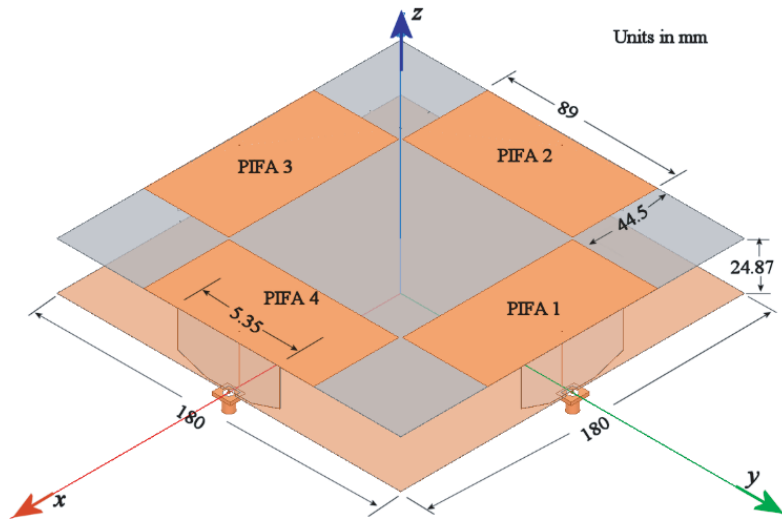


Figure 1. PIFA four elements array.

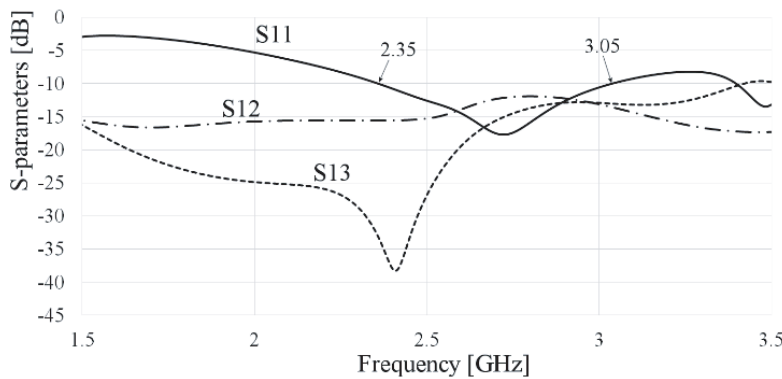


Figure 2. PIFA four elements array.

and ending at 3.05 GHz. The isolation between antennas 1 and 2 varies from 12 to 15 dB, while the one from antenna 1 to 3 reaches values of 38 dB at the lower cut-off frequency and varies to 13 dB at the upper cut-off frequency. As observed, the antennas show good isolations between elements, but the size of the array is large, presenting an area of $180 \times 180 \text{ mm}^2$. To reduce the size of the arrangement, each element is placed closer to each other, and to maximize the result of this change, the shape of the radiators is modified. Thus, the rectangle-shaped bent part of the antenna developed in [33] was modified to a trapezoidal one to optimize the use of the available space when four elements are considered around a rotation axis, as well as to avoid overlapping of the upper plates. The reduced antenna array configuration is presented in Figure 3.

Making the geometric adjustments presented in Figure 3, the plate area is reduced, and the total antenna's volume went from 805.788 mm^3 to 248.7 mm^3 . Nevertheless, as expected, the electric parameters of the antenna array were modified, which can be seen in Figure 4, where the simulated S-parameters are presented.

From Figure 4, it is observed that the bandwidth of the antenna is improved, where the lower and upper cut-off frequencies are 1.55 GHz and 2.94 GHz, respectively. However, the isolation between elements is considerably degraded. The isolation from antenna 1 to 2 is very poor from 1.55 GHz to 2.35 GHz, achieving a value lower than 10 dB. For the rest of the bandwidth, the isolation is improved, reaching values above 10 dB and a peak higher than 25 dB at 2.6 GHz.

On the other hand, the isolation determined by the S_{13} parameter shows that there is more coupling between radiators 1 and 3 than the conventional arrangement, showing values oscillating from 10 to

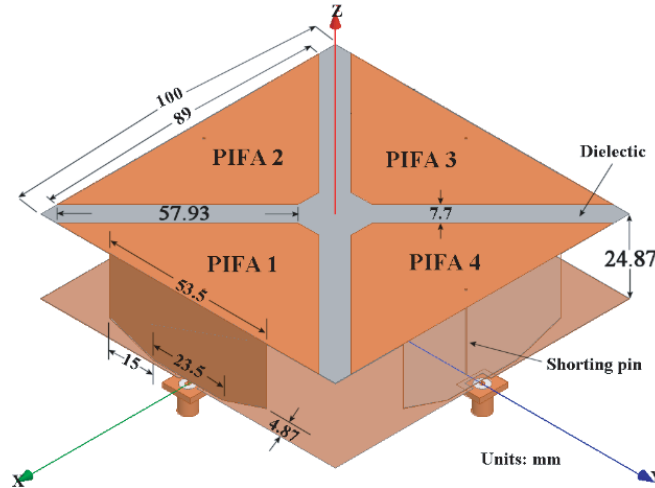


Figure 3. Reduced array configuration.

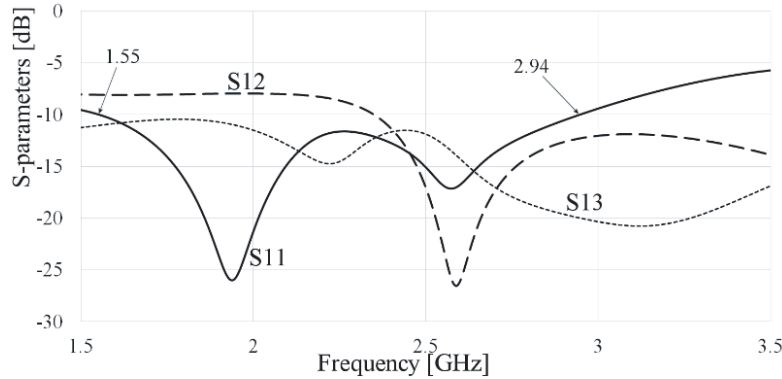


Figure 4. Simulated S parameters of the reduced antenna array.

15 dB. The poor isolation values among radiators show that the array displayed in Figure 3 are not suitable for MIMO applications. Thus, in this paper, neutralization lines (NLs) are employed to increase this parameter. The idea of using NLs in an arrangement is to cancel the effect of the adjacent radiator by feeding a signal with the same intensity and opposite phase. To optimize this phenomenon, the position of the NL is a very important parameter that must be considered.

To understand the performance of neutralization lines, Figure 5 shows the analysis of the surface current distribution of the modified array configuration when NLs are introduced. The surface current distribution analysis of each antenna was made for different NL positions, but for paper brevity, only the best performance is reported. It was determined that the addition of neutralization lines between the diagonals of adjacent top plates could invert the currents on the borders. As a result, a reduction of the effect of the electromagnetic coupling among elements is obtained. Using these neutralization lines, the design is uncomplicated compared to the techniques aforementioned and does not introduce high parasitic effects that distort the radiation characteristics [34].

The antenna array was optimized using the HFSS® software, considering inter-port coupling, bandwidth, and port matching. The position of the neutralization lines, perpendicular to the diagonals of the elements, is a primary optimization parameter. In the same way, the separation between top plates (the width of the neutralization lines) is fundamental to obtain adequate decoupling values for a MIMO system.

The surface current distribution analysis considers only the port 1 excitation since this can be extended to the other elements because they are symmetric.

In Figure 5(a), the current magnitude is plotted in contour lines. As seen, the maximum intensity

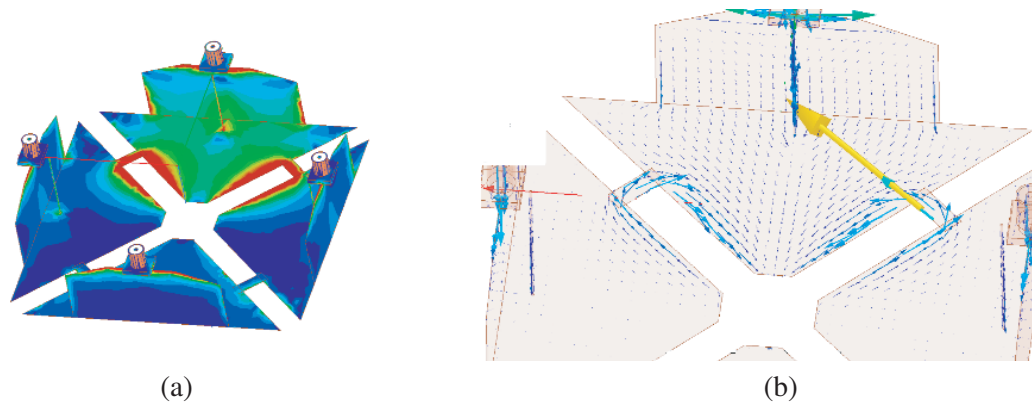


Figure 5. Currents distributions at 2.55 GHz view upside down, expressed as: (a) Contour lines, (b) vectors.

is located at port 1, where the input signal is applied. A lower magnitude is observed at port 2 and port 4 which are loaded with 50 ohms terminations. In the case of port 3, the current magnitude is the lowest among the 4 ports. This seems clear because antenna 3 is opposite to the excited antenna 1, and hence the separation is the largest in the array. On the contrary, antennas 2 and 4 are adjacent to the excited antenna, and the distance between them is smaller.

It is also observed that the neutralization lines between antennas 1 and 2, and 1 and 4 present a higher current magnitude that is better analyzed in Figure 5(b), where a detailed view of the magnitude and direction of the current near the neutralization lines are shown. Here, the currents on the borders of the top plates near the neutralization lines flow in opposite directions with similar magnitudes. This suggests that the compensatory effect takes place correctly and that the neutralization lines fulfill their function.

The separation distance is important, but the directions of the currents also contribute to the decoupling between antennas. From Figure 5(b) it is noted that the currents of antennas 2 and 4 are approximately orthogonal to the currents in antenna 1. This implicates a lower coupling between adjacent antennas. For the case of antenna 1 and antenna 4, it is observed that the currents are parallel but opposite. This also yields a lower coupling factor enforced by the higher separation distance in opposite antennas.

According to these results, the final proposal of the MIMO PIFA array is presented in Figure 6.

Next, the simulated S -parameters of the final antenna array proposal are obtained and presented in Figure 7. As presented in this figure, the antenna array shows a bandwidth from 1.8 to 3.2 GHz, approximately, given by the parameter S_{11} (parameters S_{ii} are the same). On the other hand, as observed in the same figure, the inter-port coupling is less than -10 dB over the operating bandwidth, reaching levels below -20 to -30 dB for adjacent radiators given by parameter S_{12} and the opposite radiator, specified by parameter S_{13} , respectively.

Comparing results from Figures 4 and 7, there is a big improvement, where the S_{12} parameter is enhanced by almost 6 dB, varying from -12 to -20 dB over the bandwidth. Meanwhile, the S_{13} parameter also shows improvement, obtaining values of at least -13 dB tops, and reaching values of -22 dB to -40 dB between the cut-off frequencies. The drawback of this configuration is the bandwidth reduction, showing that the lower cut-off frequency shifts up from 1.55 GHz to 1.82 GHz. Either way, the fractional bandwidth is 56% at the central frequency.

Additionally, the radiation patterns of each element are also simulated and shown in Figure 8. This figure demonstrates that the radiation pattern of each element points out to orthogonal directions compared to each other. In this way, the field correlation among antenna elements is reduced, which is a critical condition for a MIMO system with pattern diversity. In Figure 8, the excited antenna 1 generates a pattern with the maximum radiation intensity towards $-y$ -axis. If the antenna number 3 is excited, the maximum radiation intensity points out to the $+y$ -axis and complements the coverage area of antenna 1. The same can be said for antennas 2 and 4. Therefore, better coverage of the space

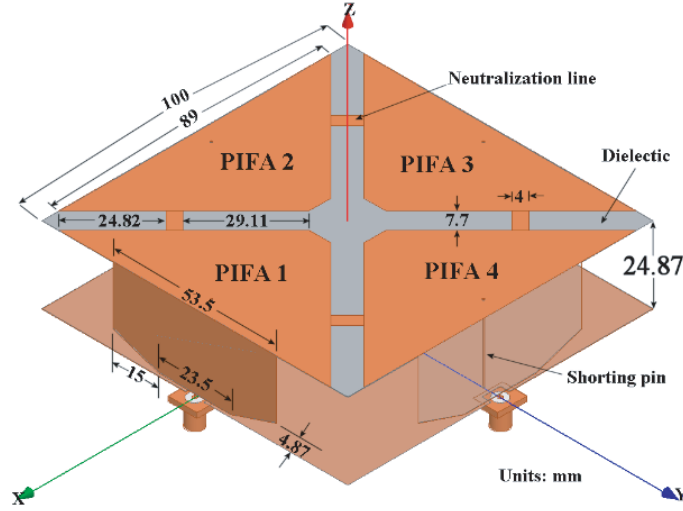


Figure 6. Antenna geometry of the PIFA array with neutralization lines.

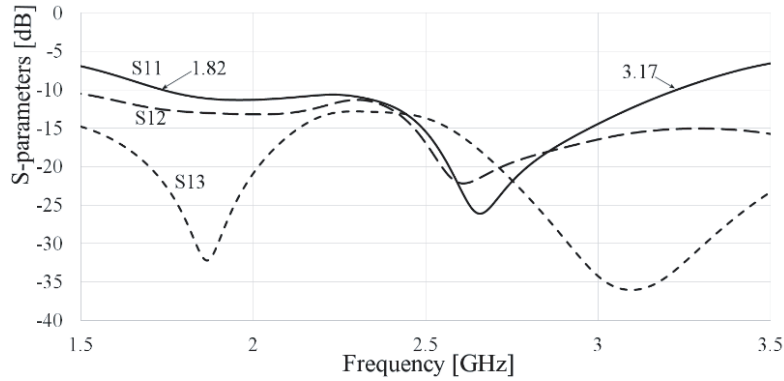


Figure 7. Simulated S parameters of the proposed array with NL.

is accomplished, and a MIMO operation with spatial diversity is enhanced.

On the other hand, to corroborate the low inter-port matching, some authors do not limit the results to the port isolation [35, 36], but also complement this parameter with the figure of merit called the Envelope Correlation Coefficient (ECC). This parameter shows how independent the antennas' radiation patterns are in a system. According to [36], the ECC can be calculated from the far-field radiation patterns as described by Eq. (1). However, authors also show a direct correlation between the expressions for the ECC based on electromagnetic fields and S -parameters as given by Eq. (2). As a result, the latter is a better and more practical option for this figure of merit.

$$ECC = \frac{\left| \iint_{4\pi} [\vec{F}_1(\theta, \varphi) \cdot \vec{F}_2(\theta, \varphi)] d\Omega \right|^2}{\iint_{4\pi} |\vec{F}_1(\theta, \varphi)|^2 d\Omega \iint_{4\pi} |\vec{F}_2(\theta, \varphi)|^2 d\Omega} \quad (1)$$

where $\vec{F}_i(\theta, \varphi)$ is the field radiation pattern of the i -th antenna when its port is excited, and \cdot denotes the Hermitian product [36].

$$ECC = \frac{|S_{11}^* S_{12} + S_{21}^* S_{22}|^2}{(1 - |S_{11}|^2 - |S_{21}|^2)(1 - |S_{22}|^2 - |S_{12}|^2)} \quad (2)$$

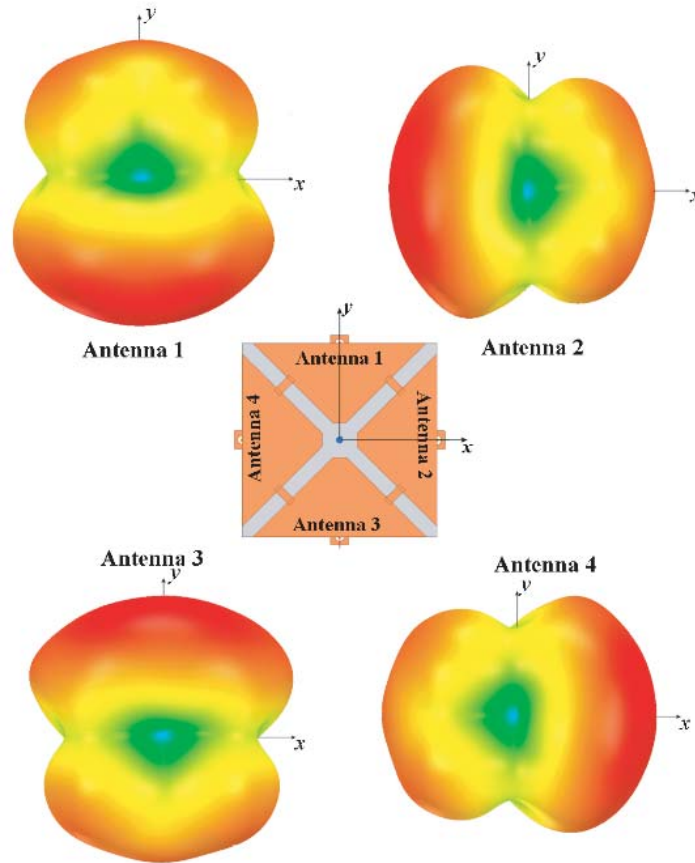


Figure 8. Three-dimensional radiation patterns of the four antennas in the array.

To compare the two methods, computer calculations of *ECC* based on far-field and *S*-parameters methods are done. According to the expression given in Eqs. (1) and (2), Figure 9 shows the *ECC* behavior between antennas 1–2 and 1–3. Because of the high computing resources needed to obtain the far-field *ECC*, only a few points are calculated. However, comparing the results from *S*-parameters and far-field simulations, similar comportment is observed, validating the use of the formula described by Eq. (2) for the *ECC*.

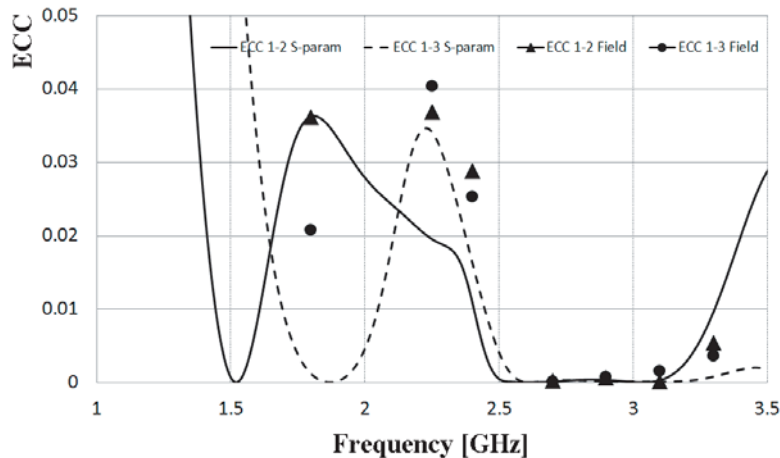


Figure 9. Envelope Correlation Coefficient considering antennas 1–2 and 1–3.

From Figure 9, it is noted that the *ECC* for antennas 1 and 2 shows a very small value, achieving no more than 0.04 at 1.8 GHz (where the maximum values are got), and for antennas 1 and 3, the value is less than 0.035 at 2.2 GHz. Meanwhile, a lower value than 0.01 at 2.55 GHz (the design frequency) for both cases (1–2 and 1–3) is obtained, showing a low correlation between adjacent and opposite antennas. This behavior is fulfilled either by the *S*-parameter equation or by the far-field procedure. According to [37], a maximum of 0.5 is required for MIMO applications, giving a great margin between desired and achieved results.

On the other hand, another figure of merit employed in space diversity systems is the diversity gain. Table 1 illustrates the simulation of this parameter at different frequencies, showing higher values over the operation bandwidth which is a great result for both relations: antenna 1 to antenna 2 and antenna 1 to antenna 3.

Table 1. Simulated diversity gain.

Frequency [GHz]	Diversity gain	Diversity gain
	Antenna 1 to 2	Antenna 1 to 3
	[dB]	[dB]
1.8	19.994	19.998
2.4	19.996	19.712
2.7	20.0	20
2.9	19.999	19.999
3.1	20.0	19.999
3.3	19.999	19.999

Finally, the Total Active Reflection Coefficient (*TARC*) is presented. This figure of merit is extremely important for evaluating the performance of a MIMO antenna over a certain bandwidth. In [38], the authors demonstrate the generalization of the *N*-ports *TARC* formula and its correct application to evaluate MIMO antennas. The equation to calculate the *TARC* is given by Eq. (3) as:

$$TARC = N^{-0.5} \sqrt{\sum_{i=1}^N \left| \sum_{k=1}^N S_{ik} e^{j\theta_{k-1}} \right|^2} \quad (3)$$

where *N* is the number of antennas in the array; *S_{ij}* are the *S*-parameters; and θ is the phase of the arriving signal to the *k*-th-1 element. For *N* = 4 elements, which is the case of this work, three variables are presented: θ_1 , θ_2 , and θ_3 . As explained in [38], θ must vary from 0° to 360°; then, taking discrete values, Eq. (3) can give as many curves as desired. For example, for five different values, there would be 125 curves. Then, to simplify the analysis and to present a clearer result, only θ_1 will vary, taking values of 0°, 90°, 180°, 225°, and 270°. The remaining variables will be set to 0°. The result of applying Eq. (3) with the specified phases is presented in Figure 10.

From Figure 10, several points must be explained. Since the *TARC* gives a more realistic behavior of the array when different signals with different phases arrive at the MIMO antenna, as observed in Figure 10, the system bandwidth changes, and it is a function of the referred phases. For example, when the *S₁₁* parameter is shown in Figure 7, the bandwidth goes from 1.82 GHz to 3.17 GHz. However, when the interaction of the other antennas is taken into account, the bandwidth changes according to the incoming signals. In Figure 10, the bandwidth keeps almost the same when the phases vary from 90° to 225°, but it is reduced when the phases are between 270° and 360°. Nonetheless, the array shows low vulnerability to random signals arriving at the radiators at the design frequency, keeping good matching from 2.48 GHz to 3.16 GHz.

3. EXPERIMENTAL RESULTS

After optimizing the antenna, the prototype was constructed and measured, and photos of the device are presented in Figure 11, showing top and bottom views.

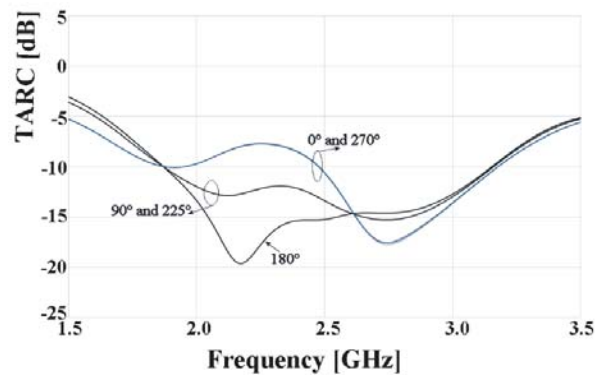


Figure 10. Total active reflection coefficient considering five values for θ_1 .

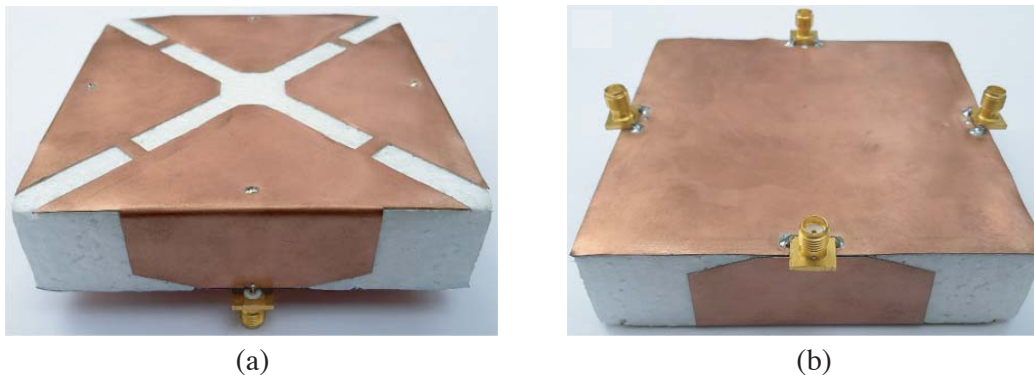


Figure 11. The prototype of the antenna array: (a) Top view and, (b) bottom view.

This prototype was designed and constructed using a low loss flexible laminate Taconic fastFilmTM27 with dielectric constant 2.7 and thickness 0.005". The ports are connected through standard SMA connectors. A block of Styrofoam is employed to provide mechanical stability to the array, in which dielectric permittivity is close to 1. To complete the construction, four short wires were welded between the top plate and the ground plane of each PIFA, using AWG 23 copper wires.

The setup in an anechoic chamber is presented in Figure 12, where two identical PIFA arrays were employed, separated 1.5 m to assure the measurements in the far-field region.

The measured S_{11} , S_{12} , and S_{13} parameters are plotted in Figure 13. The reflection coefficient is convergent to the simulated values presented in Figure 7, and the S_{12} and S_{13} parameters barely differ at some frequencies but maintain the general trend of simulated curves. In any case, the decoupling levels among radiators are below -10 dB all over the bandwidth, where large decoupling peaks can be identified at some frequencies. Specifically, S_{12} falls to -33 dB around 2.6 GHz, while S_{13} drops to -42 dB at 2.75 GHz, which are excellent levels considering the closeness of the radiators.

The gain of the antenna array was measured along the horizontal and vertical planes. To simplify the comparative analysis, only the measured gain in the vertical plane is plotted in Figure 14. The curves (a) and (b) in Figure 14 show the measured and simulated gains in this plane, respectively. Note that the measured values follow the same trend of the simulated gain curve and vary from 0 to 3 dB, approximately. However, the maximum gain is not necessarily located over a single plane. That is why the curve (c) is included to show the simulated maximum gain over the entire sphere. The simulated maximum gain values are between 1.48 dB and 5.64 dB over the 1.82–3.18 GHz band. In the same way, the total radiation efficiency was simulated and included in Figure 14 as the curve (d). The efficiency values are higher than 65%, which are acceptable for PIFA antennas [34]. As observed, the antenna gain is small, even when the antenna array presents a wide aperture. This is because a PIFA antenna presents a small gain around 3 to 5 dB, but in this case, the geometry of the radiator was changed to

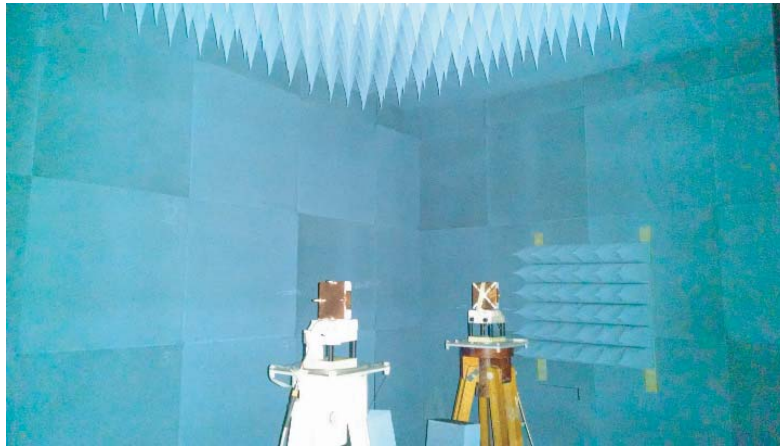


Figure 12. Measurements in the anechoic chamber.

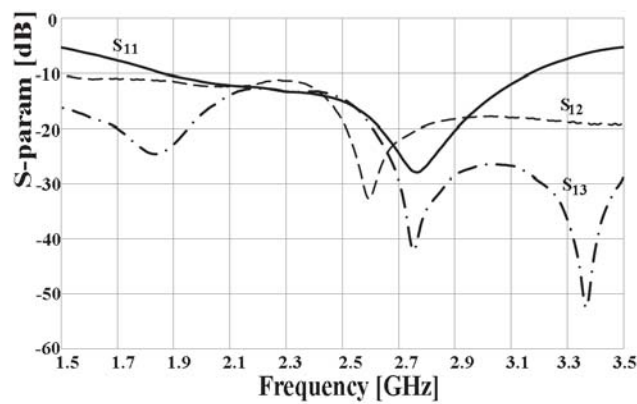


Figure 13. Measured S_{11} , S_{12} , and S_{13} parameters.

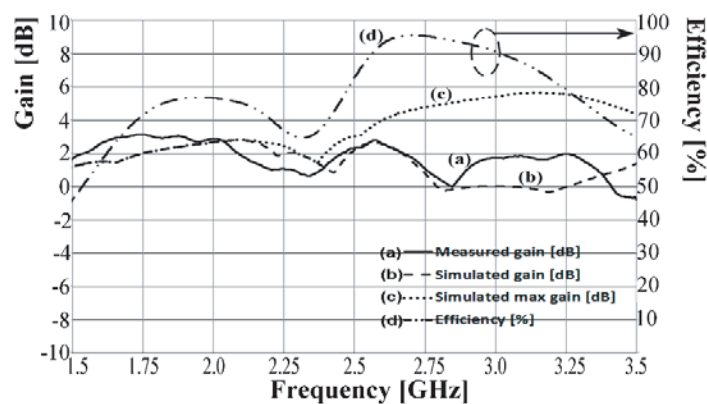


Figure 14. Different antenna parameters of each element of the array.

reduce the dimensions. For this cause, the gain is also reduced, remembering that a reduction in the antenna size directly affects either the bandwidth or the gain. In this case, the bandwidth was not considerably affected, but the gain was.

For clarity, Figure 15 shows the measured radiation pattern only for the PIFA number one at different frequencies, since the remaining antennas patterns are shaped-alike like this one, but orthogonal

to each other, whose reference can be observed in Figure 8. In Figure 15, the normalized patterns in the xy -plane, at 1.8 GHz, 2.4 GHz, and 2.7 GHz, are shown. The measured patterns are compared to simulated ones, showing great convergence for both types of data.

Finally, since the simulated results are obtained by S -parameters and far-field methods for the ECC converged, the first one is employed to obtain the measured ECC of the array. The results are presented in Figure 16. As depicted in this figure, the measured ECC for antennas 1 and 2 increases at lower frequencies in comparison to simulated results. However, as explained in [37], the requirements for MIMO applications are still fulfilled, since a value less than 0.5 is achieved, reaching 0.082 at 1.8 GHz, approximately, for antennas 1 and 2, respectively.

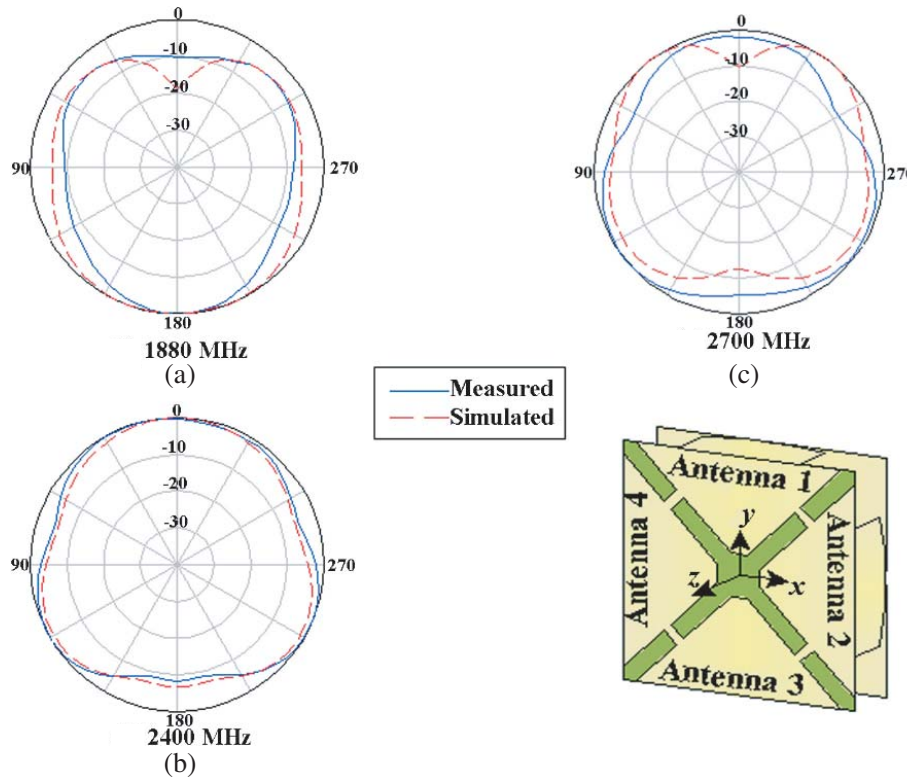


Figure 15. Radiation pattern on Antenna 1 at different frequencies in the xy -plane: (a) 1880 MHz, (c) 2700 MHz, and (b) 2400 MHz.

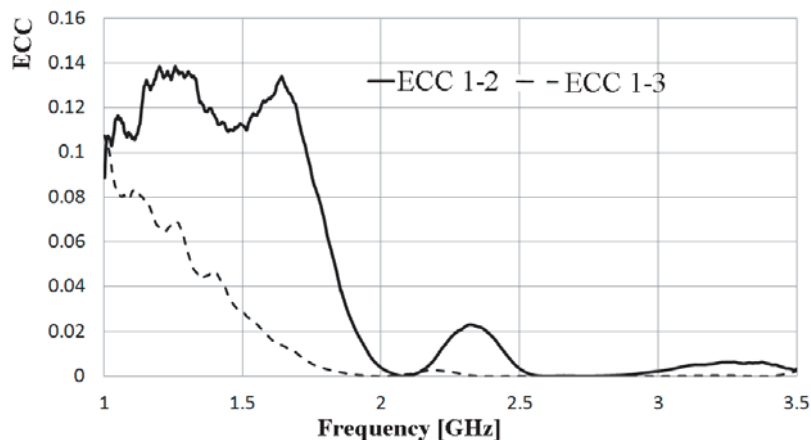


Figure 16. Measured ECC for Antenna 1 to 2 and 1 to 3.

4. CONCLUSIONS

In this work, it is demonstrated that by employing a novel configuration of a reshaped PIFA array and electrically isolated by neutralization lines, the device performs adequately for access point MIMO applications. The separation among elements is very short, reaching a distance less than $0.065\lambda_0$, at the center frequency. Using the four neutralization lines, it was possible to decouple the array elements adequately despite the very short distance of separation. One of the remarkable characteristics of the array is the wide bandwidth of the arrangement described by the S_{ii} parameters, going from 1.82 to 3.18 GHz, with acceptable inter-port decoupling levels that reach maximum values around $S_{12} = -33$ dB and $S_{13} = -42$ dB at some frequencies. Moreover, an *ECC* analysis was made considering the *S*-parameters and far-field methods, showing great convergence in results. This demonstrates that using the *S*-parameters method is good enough to observe the correlation level between ports, even for not-highly efficient antennas. Besides, the calculation of the *ECC* by this method is much more efficient, when considering the time and computer requirements. Additionally, the array shows that the radiation patterns are orthogonal to each other and cover the surrounding space in a complementary manner, a very desirable characteristic of MIMO systems. Moreover, conducting a gain diversity analysis, achieving values around 20 dB indicates the low correlation between the radiated fields among the antennas in the array. Therefore, high spatial diversity is obtained, and a correct decoupling among elements in the array is realized even when the separation of the elements is very small.

ACKNOWLEDGMENT

This work was supported by project SIP-IPN 20200330.

REFERENCES

1. Telatar, I. E., "Capacity of multi-antenna Gaussian channels," *AT & T Bell Labs*, Tech. Rep., 1995.
2. Foschini, G. J. and M. J. Gans, "On limits of wireless communications in a fading environment when using multiple antennas," *Wireless Personal Communications*, Vol. 6, No. 3, 311–335, Mar. 1998.
3. Jensen, M. A. and J. W. Wallace, "A review of antennas and propagation for MIMO wireless communication," *IEEE Transactions on Antennas and Propagation*, Vol. 52, No. 11, 2810–2824, Nov. 2004.
4. Vaughan, R. G. and J. B. Andersen, "Antenna diversity in mobile communications," *IEEE Transactions on Antennas and Propagation*, Vol. 36, No. 4, 149–172, Nov. 1987.
5. Browne, D. W., M. Manteghi, M. P. Fitz, and Yahya Rahmat-Samii, "Experiments with compact antenna arrays for MIMO radio communications," *IEEE Transactions on Antennas and Propagation*, Vol. 54, No. 11, 149–172, Nov. 2006.
6. Shiu, D. S., G. J. Foschini, M. J. Gans, and J. M. Kahn, "Fading correlation and its effect on the capacity of multielement antenna systems," *IEEE Transactions on Communications*, Vol. 48, No. 3, 502–513, Mar. 2000.
7. Balanis, C. A., *Antenna Theory: Analysis and Design*, John Wiley & Sons, New Jersey, 2005.
8. Lee, W., "Effects on correlation between two mobile radio base-station antennas," *IEEE Transactions on Communications*, Vol. 21, No. 11, 1214–1224, Nov. 1973.
9. Gupta, I. and A. Ksienski, "Effect of mutual coupling on the performance of adaptive arrays," *IEEE Transactions on Antennas and Propagation*, Vol. 31, No. 5, 785–791, Sep. 1983.
10. Janaswamy, R., "Effect of element mutual coupling on the capacity of fixed length linear arrays," *IEEE Antennas and Wireless Propagation Letters*, Vol. 1, No. 1, 157–160, 2002.
11. Wallace, J. W. and M. A. Jensen, "Mutual coupling in MIMO wireless systems: A rigorous network theory analysis," *IEEE Transactions on Wireless Communications*, Vol. 3, No. 4, 1317–1325, Jul. 2004.

12. Waldschmidt, C., S. Schulteis, and W. Wiesbeck, "Complete RF system model for analysis of compact MIMO arrays," *IEEE Transactions on Vehicular Technology*, Vol. 53, No. 3, 579–586, May 2004.
13. Svantesson, T. and A. Ranheim, "Mutual coupling effects on the capacity of multielement antenna systems," *IEEE International Conference on Acoustics, Speech, and Signal Processing (ICASSP)*, 2485–2488, Salt Lake City, USA, May 7–11, 2001.
14. Lee, W. C. Y., "Mutual coupling effect on maximum-ratio diversity combiners and application to mobile radio," *IEEE Transactions on Communication Technology*, Vol. 18, No. 6, 779–791, Dec. 1970.
15. Yang, F. and Y. R. Samii, "Microstrip antennas integrated with electromagnetic band-gap EBG structures: A low mutual coupling design for array applications," *IEEE Transactions on Antennas and Propagation*, Vol. 51, No. 10, 2936–2946, Oct. 2003.
16. Veeramani, A., A. S. Arezomand, J. Vijayakrishnan, and F. B. Zarrabi, "Compact S-shaped EBG structures for reduction of mutual coupling," *Fifth International Conference on Advanced Computing & Communication Technologies (ACCT)*, Haryana, India, Feb. 21–22, 2015.
17. Diallo, A., C. Luxey, P. Le Thuc, R. Staraj, and G. Kossiavas, "Enhanced two-antenna structures for universal mobile telecommunications system diversity terminals," *IET Microwaves, Antennas & Propagation*, Vol. 2, No. 1, 93–101, 2008.
18. Peng, H., R. Tao, W. Yin, and J. Mao, "A novel compact dual-band antenna array with high isolations realized using the neutralization technique," *IEEE Transactions on Antennas and Propagation*, Vol. 61, No. 4, 1956–1962, Apr. 2013.
19. Chen, S., Y. Wang, and S. Chung, "A decoupling technique for increasing the port isolation between two strongly coupled antennas," *IEEE Transactions on Antennas and Propagation*, Vol. 56, No. 12, 3650–3658, Dec. 2008.
20. Bhatti, R. A., S. Yi, and S. Park, "Compact antenna array with port decoupling for LTE-standardized mobile phones," *IEEE Antennas and Wireless Propagation Letters*, Vol. 8, 1430–1433, 2009.
21. Yu, Y., Y. Jiang, W. Feng, S. Mbayo, and S. Chen, "Compact multiport array with reduced mutual coupling," *Progress In Electromagnetics Research Letters*, Vol. 39, 161–168, Apr. 2013.
22. Liu, L., S. W. Cheung, and T. I. Yuk, "Compact MIMO antenna for portable devices in UWB applications," *IEEE Transactions on Antennas and Propagation*, Vol. 61, No. 8, 4257–4264, Aug. 2013.
23. Arya, A. K., A. Patnaik, and M. V. Kartikeyan, "A compact array with low mutual coupling using defected ground structures," *IEEE Applied Electromagnetics Conference (AEMC)*, Kolkata, India, Dec. 18–22, 2011.
24. Farsi, S., H. Aliakbarian, D. Schreurs, B. Nauwelaers, and G. A. E. Vandenbosch, "Mutual coupling reduction between planar antennas by using a simple microstrip U-section," *IEEE Antennas and Wireless Propagation Letters*, Vol. 11, 1501–1503, 2012.
25. Mak, A. C. K., C. R. Rowell, and R. D. Murch, "Isolation enhancement between two closely packed antennas," *IEEE Transactions on Antennas and Propagation*, Vol. 56, No. 11, 3411–3419, Nov. 2008.
26. Roshna, T. K., U. Deepak, and P. Mohanan, "Compact UWB MIMO antenna for tridirectional pattern diversity characteristics," *IET Microwaves, Antennas & Propagation*, Vol. 11, No. 14, 2059–2065, 2017.
27. Sharma, Y., D. Sarkar, K. Saurav, and K. V. Srivastava, "Three-element MIMO antenna system with pattern and polarization diversity for WLAN applications," *IEEE Antennas and Wireless Propagation Letters*, Vol. 16, 1163–1166, 2016.
28. Zhao, L. and K. Wu, "A decoupling technique for four-element symmetric arrays with reactively loaded dummy elements," *IEEE Transactions on Antennas and Propagation*, Vol. 62, No. 8, 4416–4421, Aug. 2014.

29. Boukarkar, A., X. Q. Lin, Y. Jiang, L. Y. Nie, P. Mei, and Y. Q. Yu, "A miniaturized extremely close-spaced four-element dual-band MIMO antenna system with polarization and pattern diversity," *IEEE Antennas and Wireless Propagation Letters*, Vol. 17, No. 1, 134–137, Jan. 2018.
30. Anitha, R., P. V. Vinesh, K. C. Prakash, P. Mohanan, and K. Vasudevan, "A compact quad element slotted ground wideband antenna for MIMO applications," *IEEE Transactions on Antennas and Propagation*, Vol. 64, No. 10, 4550–4553, Oct. 2016.
31. Tawk, Y., J. Costantine, and C. G. Christodoulou, "An eight-element reconfigurable diversity dipole system," *IEEE Transactions on Antennas and Propagation*, Vol. 66, No. 2, 572–581, Feb. 2018.
32. Konanur, A. S., K. Gosalia, S. H. Krishnamurthy, B. Hughes, and G. Lazzi, "Increasing wireless channel capacity through MIMO systems employing co-located antennas," *IEEE Transactions on Microwave Theory and Techniques*, Vol. 53, No. 6, 1837–1844, Jun. 2005.
33. Gomez-Villanueva, R., R. Linares-y-Miranda, J. A. Tirado-Mendez, and H. Jardon-Aguilar, "Very broadband PIFA antenna for mobile communications and ultrawideband services," *Microwave and Optical Technology Letters*, Vol. 56, No. 2, 313–316, Feb. 2014.
34. Diallo, A., C. Luxey, P. Le Thuc, R. Staraj, and G. Kossiavas, "Study and reduction of the mutual coupling between two mobile phone PIFAs operating in the DCS1800 and UMTS bands," *IEEE Transactions on Antennas and Propagation*, Vol. 54, No. 11, 3063–3074, Nov. 2006.
35. Zuo, S.-L., Y.-Z. Yin, W.-J. Wu, Z.-Y. Zhang, and J. Ma, "Investigations of reduction of mutual coupling between two planar monopoles using two $\lambda/4$ slots," *Progress In Electromagnetics Research Letters*, Vol. 19, 9–18, 2010.
36. Blanch, S., J. Romeu, and I. Corbella, "Exact representation of antenna system diversity performance from input parameter description," *Electronics Letters*, Vol. 39, No. 9, 705–707, May 1, 2003.
37. Thaysen, J. and K. B. Jakobsen, "Envelope correlation in (N, N) MIMO antenna array from scattering parameters," *Microwave and Optical Technology Letters*, Vol. 48, No. 5, 832–834, May 2006.
38. Fritz-Andrade, E., H. Jardon-Aguilar, and J. A. Tirado-Mendez, "The correct application of total active reflection coefficient to evaluate MIMO antenna systems and its generalization to N ports," *International Journal of RF and Microwave Computer-Aided Engineering*, Vol. 30, No. 4, e22113, 2020, doi: doi.org/10.1002/mmce.22113.